Topological Quantum Phase Transition in 5*d* Transition Metal Oxide Na_2IrO_3

Choong H. Kim,[1] Heung Sik Kim,[1] Hogyun Jeong,[2,3] Hosub Jin,[4] and Jaejun Yu[1,5,*]

[1]*Department of Physics and Astronomy and Center for Strongly Correlated Materials Research, Seoul National University, Seoul 151-747, Korea*

[2]*Computational Science and Technology Interdisciplinary Program, Seoul National University, Seoul 151-747, Korea*

[3]*Korea Institute of Science and Technology Information, Daejeon 305-806, Korea*

[4]*Department of Physics and Astronomy, Northwestern University, Evanston, Illinois 60208, USA*

[5]*Center for Theoretical Physics, Seoul National University, Seoul 151-747, Korea*

(Received 18 October 2011; published 5 March 2012)

We predict a quantum phase transition from normal to topological insulators in the 5*d* transition metal oxide Na_2IrO_3, where the transition can be driven by the change of the long-range hopping and trigonal crystal field terms. From the first-principles-derived tight-binding Hamiltonian, we determine the phase boundary through the parity analysis. In addition, our first-principles calculations for Na_2IrO_3 model structures show that the interlayer distance can be an important parameter for the existence of a three-dimensional strong topological insulator phase. Na_2IrO_3 is suggested to be a candidate material which can have both a nontrivial topology of bands and strong electron correlations.

DOI: 10.1103/PhysRevLett.108.106401 PACS numbers: 71.70.Ej, 73.20.−r, 73.43.Nq

Topological insulators are newly discovered materials with a bulk band gap and topologically protected metallic surface states [1,2]. The theoretical predictions on Bi-based topological insulators, such as Bi_xSb_{1-x}, Bi_2Se_3, and Bi_2Te_3 [3,4], have been experimentally realized [5–8]. The search for topological insulators has been extended to ternary Heusler [9] and chalcogenide compounds [10], but they are still limited to either the narrow or zero gap semiconductors. Recently, the layered honeycomb lattice Na_2IrO_3 [11] and pyrochlore $A_2Ir_2O_7$ [12,13] have been suggested as possible topological insulators, although topological insulators with transition metal *d* electrons have not been fully investigated. Contrary to the *s*-*p* electron systems, transition metal oxides with localized *d* electrons are expected to have both strong on-site Coulomb interactions and spin-orbit couplings. In particular, 5*d* transition metal oxides such as iridates have a relatively weaker Coulomb correlation competing with spin-orbit-coupled band structures.

The interplay between the nontrivial band topology and the electron correlation effect can be an interesting development in the study of topological insulators. Ir-based transition metal oxides have shown some noble physics, such as the $j_{\text{eff}} = 1/2$ insulating state in Sr_2IrO_4 [14–16], the anomalous metal-insulator transition in $A_2Ir_2O_7$ [17], and the spin-liquid state in $Na_4Ir_3O_8$ [18], where both spin-orbit coupling and correlation play important roles.

Na_2IrO_3 [19,20] has been proposed as a layered quantum spin Hall (QSH) insulator. Assuming the $j_{\text{eff}} = 1/2$ character of the band near the Fermi level [11], a single-band tight-binding model for the Ir-O layer is mapped to the Kane-Mele model [1] for the QSH effect. The proposed model Hamiltonian is, however, inconsistent with the first-principles band structure result which leads to a different prediction on the band topology of Na_2IrO_3 [21]. The inconsistency is partly due to the structural parameters used for the first-principles calculations. It implies that its band topology may be sensitive to the structural variation. Consequently, a small change of structure or interaction strength can drive a quantum phase transition, e.g., the change of its topological character. To understand the basic physics determining the band topology of Na_2IrO_3, we need to clarify the topological character of the spin-orbit-coupled ground state and its dependence on the structure and interaction strength.

In this Letter, we present a quantum phase transition between topological insulators (TIs) and normal insulators (NIs) in Na_2IrO_3 based on an effective tight-binding Hamiltonian. We derived the effective Hamiltonian from the realistic tight-binding description of first-principles band structures. The electronic structure of the planar edge-shared IrO_6 octahedra contains large trigonal crystal field and direct hopping terms as well as a significant long-range hopping between extended Ir 5*d* orbitals. The phase boundary between topological and normal insulating phases is shown to depend on both the trigonal crystal field and the long-range hopping in Na_2IrO_3. From the first-principles calculations of model structures, which simulate the change of tight-binding parameters, we confirmed that the interlayer distance can play a crucial role in the determination of the three-dimensional strong TI in Na_2IrO_3.

We introduce a tight-binding (TB) model for Na_2IrO_3 from the results of first-principles calculations [22]. The model is based on the Ir t_{2g} manifold in the two-dimensional honeycomb lattice and incorporates parameters for an indirect hopping through the oxygen 2*p* orbital (t_{pd}), two kinds of direct hopping between neighboring Ir atoms (t_{dd_1} and t_{dd_2}), and another indirect hopping

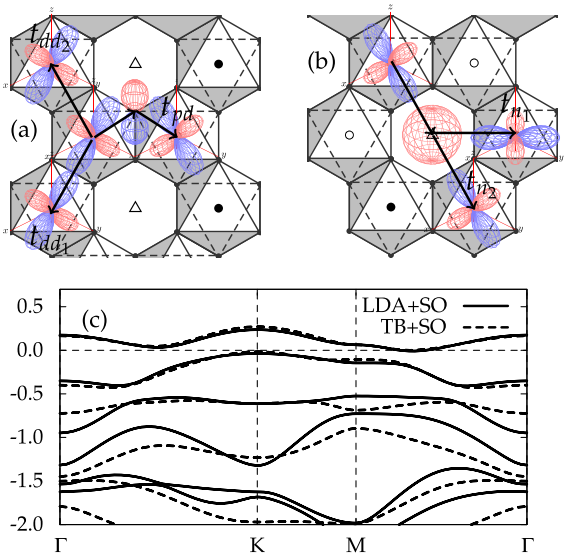

FIG. 1 (color online). Hopping parameters considered in our tight-binding model: (a) the indirect hopping (t_{pd}) mediated by the oxygen $2p$ orbital and two kinds of direct hoppings (t_{dd_1} and t_{dd_2}), (b) the second-nearest-neighbor hopping (t_{n_1}) and the third-nearest-neighbor hopping (t_{n_2}), and (c) the band structure of first-principles (solid lines) and tight-binding (dashed lines) calculations with spin-orbit coupling.

through the sodium $3s$ orbital (t_n), as illustrated in Figs. 1(a) and 1(b). It is noted that the indirect hopping through the sodium $3s$ orbital of Fig. 1(b) makes the second- and third-nearest-neighbor hopping terms non-negligible and plays a crucial role in the determination of the topology of the band structure. In addition, we take into account both trigonal crystal field Δ and spin-orbit coupling (SOC) λ terms. The TB parameters are summarized in Table I. The energy unit is in eV. The values of the parameters are fitted to the results of density-functional-theory (DFT) calculations within the local density approximation (LDA). For the DFT calculations, we used the DFT code, OPENMX [23], based on the linear-combination-of pseudo-atomic-orbitals method [24]. The SOCs were included via the relativistic j-dependent pseudopotential scheme in the noncollinear DFT formalism [25–27]. The unit cell we used in the DFT calculations is a simplified version of the original crystal, where the c-axis periodicity is reduced by changing the relative stacking of Na layers with respect to the Ir network and also by neglecting the distortion of oxygen octahedra. We have checked the band structures with the different stacking of Na layers and the rotation of oxygen atoms around the axis perpendicular to the plane and observed only a small change in the band dispersion and fitting parameters. Our TB model describes well the DFT band structure, especially the bands near the Fermi level (E_F), as shown in Fig. 1(c).

TABLE I. Values of tight-binding parameters (in eV) obtained from the first-principles band structure.

Parameters	Character	Value (eV)
t_{pd}	$(pd\pi)^2/(\epsilon_d - \epsilon_p)$	0.25
t_{dd_1}	$\frac{3}{4}(dd\sigma) + \frac{1}{4}(dd\delta)$	−0.5
t_{dd_2}	$\frac{1}{2}(dd\pi) + \frac{1}{2}(dd\delta)$	0.15
t_n	$(sd\sigma)^2/(\epsilon_d - \epsilon_s)$	−0.075
Δ	$E_{e'_g} - E_{a_{1g}}$	0.6
λ	Spin-orbit coupling	0.5

It is interesting that the calculated parity invariants and Z_2 topological numbers for our TB model depend critically on the second- and third-nearest-neighbor hopping term t_n, as demonstrated in Table II. The topological invariants were determined by following the method proposed by Fu and Kane [28]. The Z_2 topology of the DFT band structure with $t_n = -0.075$ turns out to be trivial. This result is consistent with the previous first-principles calculations result [21], contrary to the quantum spin Hall insulator phase predicted by Shitade *et al.* [11]. This discrepancy is likely due to an oversimplification of the tight-binding model employed in Ref. [11]. Their model was based on the assumption that the low-energy degrees of freedom are determined by the half-filled $j_{\text{eff}} = 1/2$ doublets. However, when the significant trigonal crystal field is introduced in Na_2IrO_3, $j_{\text{eff}} = 1/2$ and $j_{\text{eff}} = 3/2$ are not well separated and the $j_{\text{eff}} = 1/2$ doublets no longer serve as a useful basis [21]. The extended nature of the $5d$ orbital combined with the edge-shared octahedral structure in the $Ir_{2/3}Na_{1/3}O_2$ plane of Na_2IrO_3 is a source of such a strong trigonal crystal field.

The topological character of Na_2IrO_3 is quite sensitive to the magnitude of t_n. By turning off the second- and third-nearest-neighbor hoppings, i.e., $t_n = 0$, the system becomes a nontrivial TI with $\nu = 1$. The tiny difference in the magnitude of t_n is responsible for the inversion of the valance and conduction bands, thereby leading to the change of the $\delta(M)$ sign. It indicates that t_n is a key control parameter for the "band inversion" in this system. Therefore, the TB model with the nearest-neighbor hoppings only cannot be sufficient for the description of the topological character of Na_2IrO_3, even though the nearest-neighbor TB models can describe reasonably the band dispersions of the $j_{\text{eff}} = 1/2$ states in Sr_2IrO_4 [14,16] and the hyper-Kagome $Na_4Ir_3O_8$ [29,30].

The nontrivial (trivial) Z_2 topological number can also be confirmed by the odd (even) number of pairs of gapless

TABLE II. Parity invariants $\delta(\Gamma_i)$ and Z_2 topological invariants (ν) with and without t_n, as determined from the product of parity eigenvalues at each time-reversal-invariant momentum Γ, M_1, M_2, and M_3.

	$\delta(\Gamma)$	$\delta(M_1)$	$\delta(M_2)$	$\delta(M_3)$	$Z_2(\nu)$
$t_n = -0.075$	−1	−1	−1	−1	0
$t_n = 0$	−1	1	1	1	1

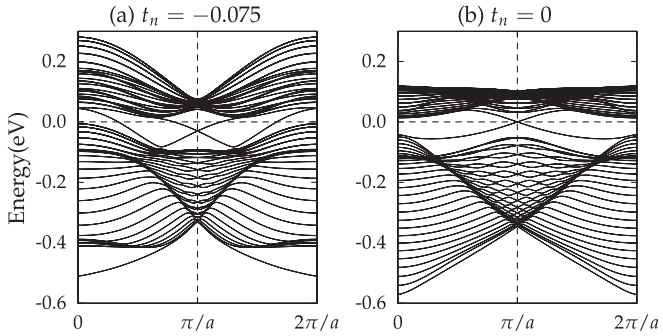

FIG. 2. One-dimensional energy bands for armchair strip in the (a) NI phase with $t_n = -0.075$ and (b) TI phase with $t_n = 0$.

edge states. To examine the edge states, we constructed a TB Hamiltonian for the strip geometry with two edges in an armchair configuration. Figure 2 shows the one-dimensional energy bands with $t_n = -0.075$ and $t_n = 0$. The bulk states and gaps are clearly seen, and there are edge states which transverse the gap. In the normal insulating phase ($\nu = 0$), the edge states cross the Fermi energy an even number of times, as expected from the trivial Z_2 topological number.

Transitions between trivial and nontrivial phases can be tuned by adjusting the key parameters of the band structure. Murakami and co-workers [31] developed the low-energy effective theory for the phase transition between TI and NI systems in 2D and discussed the classification of the possible types of transition. Following their classification, the gap closing at the time-reversal-invariant momenta ($\mathbf{k} = \mathbf{G}/2$) occurs in systems with inversion symmetry. In our model, t_n controls the gap closing at the M point in the Brillouin zone, contrary to the case of a honeycomb lattice model such as the Kane-Mele model, where the gap closes at the K and K' points. The low-energy long-wavelength effective Hamiltonian, which is expanded to linear order in k around the M point, can be written as

$$H(\mathbf{k}) = E_0 + \begin{pmatrix} m & z_- & & \\ z_+ & -m & & \\ & & m & -z_+ \\ & & -z_- & -m \end{pmatrix}, \qquad (1)$$

where $\mathbf{k}' = \mathbf{k} - M$ and $z_\pm = b_1 k'_x + b_3 k'_y \pm i b_2 k'_y$, with real constants b_1, b_2, and b_3 [31]. Since the eigenenergies $E = E_0 \pm \sqrt{m^2 + z_+ z_-}$, $m = 0$ corresponds to the gap closing.

Figure 3 shows the TB band structure along some high-symmetry line for the several values of t_n. In the TI region ($t_n = 0$), the valance and conduction bands are separated by a finite gap with negative mass. When $|t_n|$ increases, the direct gap at the M point decreases. Finally, the gap collapses at the transition point $t_n \simeq -0.021$. As $|t_n|$ passes through the transition point, the gap reopens and the system becomes a normal insulator with positive mass. During this procedure, the order of the bands is inverted around the M point, which characterizes the topological nature of the system.

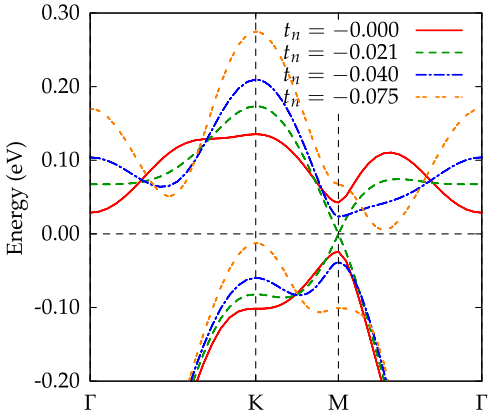

FIG. 3 (color online). TB band structure with the variation of t_n. The solid (red) ($t_n = 0$) lines belong to the TI, and the dot-dashed (blue) ($t_n = -0.040$) and double-dashed (orange) ($t_n = -0.075$) lines belong to the NI. Note that, at the transition point, i.e., $t_n = -0.021$, the dispersion is linear.

To further verify the relation between the mass and the control parameters, we obtain the expression for the mass as a function of t_n, Δ, and SOC (λ):

$$2m = A + B\Delta + Ct_{n_1} - 2t_{n_2} + D\Delta t_{n_1}. \qquad (2)$$

Here, to clarify the role of second- and third-nearest hoppings, we refined t_n into the second-nearest-neighbor hopping, t_{n_1}, and the third-nearest-neighbor hopping, t_{n_2}. The expansion coefficients A, B, C, and D can be represented as functions of λ. In the range of λ from $0.8\lambda_0$ to $1.6\lambda_0$, where λ_0 is the SOC determined by the LDA calculation, the coefficients can be fitted as follows:

$$\begin{aligned} A &= +0.0746 - 0.1438\lambda, \\ B &= -0.0237 - 0.3061\lambda + 0.2587\lambda^2, \\ C &= -2.2178 + 1.2660\lambda, \\ D &= +1.0975 - 0.6837\lambda. \end{aligned} \qquad (3)$$

In the limiting cases of $\lambda/\lambda_0 = 1$ and ∞, the coefficients are also shown in Table III. From Eq. (2), we can determine the Z_2 topological number of the system for given t_n, Δ, and λ by checking the sign of mass. This mass function correctly characterizes the topological phase transition.

TABLE III. The expansion coefficients of mass function in Eq. (2) when $\lambda/\lambda_0 = 0$ and ∞. These coefficients at $\lambda/\lambda_0 = 1$ and $\Delta = 0.6$ correctly describe the transition point $t_n \simeq -0.021$.

λ/λ_0	A	B	C	D
1	−0.00	−0.12	−1.61	0.58
∞	−0.13	−0.00	−0.13	0.00

Figure 4 shows a $\lambda - t_n$ phase diagram for several values of Δ. For a sufficiently large λ, an indirect bulk gap opens and the system becomes an insulator. The insulating region is divided into two phases: TI and NI. The phase boundary between TI and NI corresponds to the $m = 0$ line. There seems to be an asymptotic limit of t_n beyond which the system stays as a normal insulator regardless of the strength of the SOC λ. The vertical dashed line in Fig. 4 is described by

$$t_n = \frac{A}{C-2} \approx -0.067 \tag{4}$$

with $\Delta = 0.6$. This implies that an arbitrarily large SOC cannot guarantee the nontrivial topology, even if the upper four bands originate from the $j_{\text{eff}} = 1/2$ states.

Another important factor controlling the topological character is the trigonal crystal field, Δ. In fact, both SOC and the trigonal crystal field are two competing parameters characterizing the bands near the Fermi level. While SOC prefers the formation of the $j_{\text{eff}} = 1/2$ state, the large trigonal crystal field becomes an obstacle for the $j_{\text{eff}} = 1/2$ state. In this system, however, the trigonal crystal field seems to play a crucial role. As far as $B < 0$ and $D > 0$ of Eq. (2), as shown in Table III, it is clear that a large trigonal crystal field is in favor of the nontrivial topology. This trend in the parameter dependence of the topological character is clearly reflected in the phase diagram of Fig. 4.

Returning to a realistic system of Na_2IrO_3 materials, we tried to probe possible TI phases by performing first-principles calculations. According to the simulated TB parameters for the TI phase, we choose two representative structures among the various structures: (i) the original geometry of Na_2IrO_3 ($c/c_0 = 1.0$) and (ii) a virtual structure with the interlayer distance expanded by 30% ($c/c_0 = 1.3$). Calculated Z_2 topological numbers for each configuration are as listed in Table IV. Here, the c/c_0 parameter represents the change of interlayer distance relative to the original one. It is remarkable to find a nontrivial Z_2 number for the structure with $c/c_0 = 1.3$. In other words, the increased interlayer distance drives the NI into the TI. To understand the change of electronic structure between $c/c_0 = 1.0$ and $c/c_0 = 1.3$, we constructed the maximally localized Wannier function (MLWF) [32,33] and obtained the MLWF effective Hamiltonian. It is found that the trigonal crystal field enhanced by the increase of interlayer distance contributes to the change of Z_2 character for Na_2IrO_3. When we increase the interlayer distance, the energy level of the interplane Na $3s$ state lowers. The second- or higher-order hoppings through the unoccupied $3s$ state of interplane Na contribute to the on-site Hamiltonian matrix elements. Since these matrix elements give rise to the energy separation between e_g' and a_{1g} states, it can be interpreted that the trigonal crystal field contributes to the band inversion at the M point. In fact, the band inversion occurs only at three M points in the $k_z = 0$ plane. However, as shown in Table IV, the parity invariants $\delta(\Gamma_i)$ for $c/c_0 = 1.3$ are quite different for the $k_z = 0$ and $k_z = \pi$ planes. It indicates that the c-axis hopping is also important for the existence of the TI phase in the three-dimensional system of Na_2IrO_3.

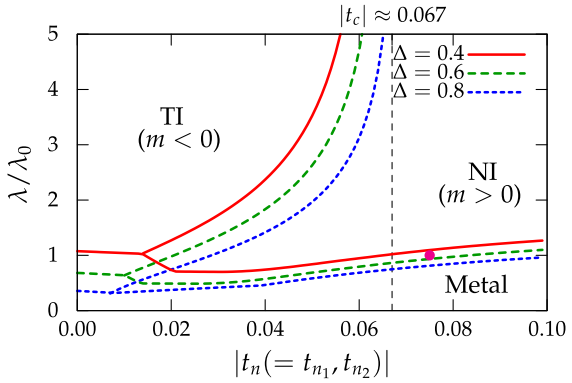

FIG. 4 (color online). Phase diagram as a function of t_n and SOC for several values of Δ. The pink circle indicates where the reality exists. $|t_c| = 0.062$ is the asymptotic line in the case of $\Delta = 0.6$.

In conclusion, we provide a microscopic picture for the topological phase diagram in Na_2IrO_3 and identify the key control parameters based on the effective Hamiltonian analysis. We predict that the TI phase of Na_2IrO_3 can be realized by controlling the long-range hopping and trigonal crystal field terms. Our first-principles calculations for the simulated Na_2IrO_3 model structure suggest that the interlayer distance can play a crucial role in the determination of a three-dimensional strong TI. In practice, we propose two ways of driving a transition from NI to TI: (i) epitaxial strain by the substitution of Na by other elements such as Li or a film growing on an appropriate substrate or (ii) intercalation of some molecules for the increase of the interlayer distance (e.g., is the water-intercalated $Na_{0.35}CoO_2 \cdot 1.3H_2O$ showing the superconductivity? [34]). Indeed our first-principles calculations demonstrate that the topological insulator phase of Li_2IrO_3 can be achieved by 2% in-plane lattice strain [35]. In addition, other structure manipulation techniques developed for superlattice and heterostructure may be adopted to control the NI-to-TI transition and to design the topological-insu-

TABLE IV. Parity invariants $\delta(\Gamma_i)$ and Z_2 topological invariants calculated from first-principles calculations. We considered two different structures: (i) the original geometry of Na_2IrO_3 ($c/c_0 = 1.0$) and (ii) a virtual structure with the interlayer distance enlarged by 30% ($c/c_0 = 1.3$).

	$\delta(\Gamma)$	$\delta(M)$	$\delta(A)$	$\delta(L)$	$\nu;(\nu_1\nu_2\nu_3)$
$c/c_0 = 1.0$	-1	-1	-1	-1	0; (000)
$c/c_0 = 1.3$	-1	1	-1	-1	1; (000)

lator-based devices. A recent experiment observed an antiferromagnetic (AFM) insulating behavior in Na_2IrO_3 [19,20]. The AFM ordering in the TI phase of Na_2IrO_3 can be a candidate of a topological magnetic insulator [36,37] or a topological Weyl semimetal [38] below ordering temperature (T_N). Above T_N, correlations could enhance the SOC effects due to the suppression of effective bandwidth to stabilize the TI phase [12]. Further, there are proposals for the topological Mott insulator having gapless surface spin-only excitations [11,12]. Na_2IrO_3 is likely to provide a new playground to study the effect of the correlation in TI.

This work was supported by the NRF through the ARP (R17-2008-033-01000-0). We also acknowledge the support from KISTI under the Supercomputing Application Support Program.

*Corresponding author.
jyu@snu.ac.kr

[1] C. L. Kane and E. J. Mele, Phys. Rev. Lett. **95**, 146802 (2005).
[2] B. A. Bernevig, T. L. Hughes, and Shou-Cheng Zhang, Science **314**, 1757 (2006).
[3] L. Fu, C. L. Kane, and E. J. Mele, Phys. Rev. Lett. **98**, 106803 (2007).
[4] H. Zhang *et al.*, Nature Phys. **5**, 438 (2009).
[5] Koenig *et al.*, Science **318**, 766 (2007).
[6] D. Hsieh *et al.*, Nature (London) **452**, 970 (2008).
[7] Y. Xia *et al.*, Nature Phys. **5**, 398 (2009).
[8] Y. L. Chen *et al.*, Science **325**, 178 (2009).
[9] S. Chadov *et al.*, Nature Mater. **9**, 541 (2010); H. Lin *et al.*, *ibid.* **9**, 546 (2010).
[10] H. Lin *et al.*, Phys. Rev. Lett. **105**, 036404 (2010); B. Yan *et al.*, Europhys. Lett. **90**, 37 002 (2010); H. Jin, J.-H. Song, A. J. Freeman, and M. G. Kanatzidis, Phys. Rev. B **83**, 041202(R) (2011).
[11] A. Shitade *et al.*, Phys. Rev. Lett. **102**, 256403 (2009).
[12] D. Pesin and L. Balents, Nature Phys. **6**, 376 (2010).
[13] B. J. Yang and Y. B. Kim, Phys. Rev. B **82**, 085111 (2010).
[14] B. J. Kim *et al.*, Phys. Rev. Lett. **101**, 076402 (2008).
[15] B. J. Kim *et al.*, Science **323**, 1329 (2009).
[16] H. Jin, H. Jeong, T. Ozaki, and J. Yu, Phys. Rev. B **80**, 075112 (2009).
[17] K. Matsuhira *et al.*, J. Phys. Soc. Jpn. **76**, 043706 (2007).
[18] Y. Okamoto, M. Nohara, H. Aruga-Katori, and H. Takagi, Phys. Rev. Lett. **99**, 137207 (2007).
[19] Y. Singh and P. Gegenwart, Phys. Rev. B **82**, 064412 (2010).
[20] X. Liu *et al.*, Phys. Rev. B **83**, 220403(R) (2011).
[21] H. Jin *et al.*, arXiv:0907.0743.
[22] See Supplemental Material at http://link.aps.org/supplemental/10.1103/PhysRevLett.108.106401 for details of the tight-binding model.
[23] The OPENMX (Open source package for Material eXplorer) software package for nanoscale material simulations, http://www.openmx-square.org.
[24] T. Ozaki, Phys. Rev. B **67**, 155108 (2003).
[25] A. H. MacDonald and S. H. Vosko, J. Phys. C **12**, 2977 (1979).
[26] G. B. Bachelet, D. R. Hamann, and M. Schlüter, Phys. Rev. B **26**, 4199 (1982).
[27] G. Theurich and N. A. Hill, Phys. Rev. B **64**, 073106 (2001).
[28] L. Fu and C. L. Kane, Phys. Rev. B **76**, 045302 (2007).
[29] M. R. Norman and T. Micklitz, Phys. Rev. B **81**, 024428 (2010).
[30] D. Podolsky and Y. B. Kim, Phys. Rev. B **83**, 054401 (2011).
[31] S. Murakami, S. Iso, Y. Avishai, M. Onoda, and N. Nagaosa, Phys. Rev. B **76**, 205304 (2007).
[32] N. Marzari and D. Vanderbilt, Phys. Rev. B **56**, 12 847 (1997).
[33] H. Weng, T. Ozaki, and K. Terakura, Phys. Rev. B **79**, 235118 (2009).
[34] K. Takada *et al.*, Nature (London) **422**, 53 (2003).
[35] Heung Sik Kim *et al.* (unpublished).
[36] R. Li *et al.*, Nature Phys. **6**, 284 (2010).
[37] J. Wang, R. Li, S.-C. Zhang, and X.-L. Qi, Phys. Rev. Lett. **106**, 126403 (2011).
[38] X. Wan, A. M. Turner, A. Vishwanath, and S. Y. Savrasov, Phys. Rev. B **83**, 205101 (2011).